

CHAPTER 1

BATTERY LIFETIME ESTIMATION AND OPTIMIZATION FOR UNDERWATER SENSOR NETWORKS

Raja Jurdak

School of Information and Computer Science
Center for Pervasive Communications and Computing
University of California, Irvine CA 92697

Cristina Videira Lopes

School of Information and Computer Science
Center for Pervasive Communications and Computing
University of California, Irvine CA 92697

Pierre Baldi

School of Information and Computer Science

California Institute for Telecommunications and Information Technology Cal-(IT)²
University of California, Irvine CA 92697



A JOHN WILEY & SONS, INC., PUBLICATION

1.1 ABSTRACT

Acoustic technology has been established as the exclusive technology that provides robust underwater communications for military and civilian applications. One particular civilian application of interest is the deployment of underwater acoustic sensor networks. The main challenges of deploying such a network are the cost and the limited battery resources of individual sensor nodes. Here, we provide a method that addresses these challenges by estimating the battery lifetime and power cost of shallow water networks, in terms of four independent parameters: (1) internode distance; (2) transmission frequency; (3) frequency of data updates; and (4) number of nodes per cluster. Because transmission loss in water is dependent on both frequency and distance, we extend the general method to exploit topology-dependent distance and frequency assignments. We use the method to estimate the battery life for tree, chain, and grid topologies for various combinations of internode distance, frequency and cluster size in a shallow water setting. The estimation results reveal that topology-dependent assignments prolong battery life of the tier-independent method by a factor of 1.05 to 131 for large networks. In the case of a linear network deployed along a coastline with a target battery life of 100 days, topology-dependent assignments could increase the network range and aggregated sensor data of the topology-independent method by a factor of 3.5.

1.2 INTRODUCTION

Underwater acoustic communication has been used for a long time in military applications. Compared to radio waves, sound has superior propagation characteristics in water, making it the preferred technology for underwater communications. The military experience with this technology has led to increased interest for civilian applications, including the development of underwater networks. The main motivation for underwater acoustic networks is their relative ease of deployment since they eliminate the need for cables and they do not interfere with shipping activity. These networks are useful for effectively monitoring the underwater medium for military, commercial or environmental applications. Environmental applications include monitoring of physical indicators [1] (such as salinity, pressure, and temperature) and chemical/biological indicators (such as bacteria levels, contaminant levels, and dangerous chemical or biological agent levels in reservoirs and aqueducts).

The work presented in this paper is part of an interdisciplinary effort at UCI to develop a shallow water underwater sensor network for real-time monitoring of environmental indicators, similar to current air quality monitoring systems. One of the major considerations for the development of such a network is the power consumption at individual nodes. This work is motivated by the practical need to estimate the battery life of sensor nodes, which has implications on the usefulness, topology and range of the network. Estimating the battery life of sensor networks prior to design and deployment of the actual network requires an analytical method which coarsely captures the behavior of a shallow water sensor network. On the theoretical level, this work is driven by the need to develop a generic method for battery lifetime estimation that combines both the networking and medium-specific aspects in sensor networks.

Most of the existing work has focused on modeling the battery lifetime of sensor networks in air [2,3], including the papers in this section of the book. The goals of this work are:

- To provide an estimation method for network battery lifetime specific to the conditions of underwater acoustic sensor networks
- To propose topology-dependent optimizations for power consumption
- To use the estimation method to evaluate the benefits of the optimizations for a typical shallow water sensor network

The remainder of the paper is as follows. Section 1.3 provides the necessary background and reviews previous related work that addresses the network lifetime issue. Section 1.4 introduces the steps of the estimation method. Section 1.5 presents the topology-specific optimizations for power consumption. Section 1.6 uses the method to estimate the battery life and power consumption of two topologies that are representative of shallow water network scenarios. Section 1.7 discusses the estimation results and concludes the paper.

1.3 RELATED WORK

Interest in underwater acoustics dates back to the early 20th century when sonar waves were used to detect icebergs [4]. Later, the military started using underwater acoustics for detecting submarines [4] and mines [5,6]. Underwater acoustic applications further extended to seafloor imaging [7], object localization and tracking [8], and data communication [4] for ocean exploration and management of coastal areas. The previous experiences with underwater acoustics have led to the design of underwater sensor networks that include a large number of sensors and perform long term monitoring of the underwater environment [9]. In underwater sensor networks, the issue of limited battery resources at the sensors is particularly important because of the difficulty and cost of recharging sensor batteries once the network is deployed.

In the recent literature, several approaches address estimation and optimization of the lifetime of energy-constrained networks. In the context of underwater networks, Fruehauf and Rice [10] propose the use of steerable directional acoustic transducers for signal transmission and reception in underwater nodes to reduce the energy consumption and thus prolong the lifetime of a node. Among other approaches that apply to more general energy-constrained networks, Tilaky et al. [11] assess the tradeoffs involved in the design and topology of sensor networks. Marsan et al. [12] consider techniques to maximize the lifetime of a Bluetooth network by optimizing network topology, and argue that their optimization techniques are also applicable to general ad hoc networks. Several routing [13–16] and MAC [17] algorithms have been developed for energy efficient behavior in sensor network in order to maximize network lifetime. For example, Misra and Banerjee [13] present a routing algorithm to maximize network lifetime by choosing routes that pass through nodes with currently high capacity. The capacity of a node according to [13] is a combined measure of the remaining battery energy and the estimated energy spent in reliably forwarding data of other nodes in the network. Panigrahi et

al. [18] derive stochastic models for battery behavior to represent realistic battery behavior in mobile embedded systems. In our work, we model battery behavior as a function of the acoustic transmit and receive power, which are the dominant sources of power consumption in underwater transceivers [19]. Some models [2, 3] attempt to derive an upper bound on the lifetime of a sensor network, in terms of a generic set of parameters. Some of the parameters in our method, such as the internode distance and the number of nodes that relay data to the sink, are also considered in [2] and [3]. However, both of the previous models assume a path loss inversely proportional to d^n , where d is the distance between a sender and receiver. This assumption applies to most aerial wireless networks, but does not capture the specific conditions of underwater networks, in which the path loss depends on frequency as well as distance (see Equations 1.3-1.4 below). Furthermore, delay and multi-path propagation effects in underwater networks are certainly different from aerial networks. The case of relatively infrequent data updates is addressed in [20], which focuses on radio frequency sensor networks where nodes periodically send data updates towards the central node. In our method, we also consider the case of infrequent data updates towards a central node in underwater acoustic networks, and as in [20], we attempt to derive algorithms for data gathering and aggregation that maximize the lifetime of the network.

1.4 NETWORK BATTERY LIFE ESTIMATION METHOD

The challenges of designing shallow water acoustic networks include the following:

1. Spectrum allocation: the limited available acoustic spectrum [21] in underwater environments makes this issue particularly challenging.
2. Topology: internode distances and number of forwarding nodes are factors that impact the overall performance of the network [12] [20] [2].
3. Shallow water environment: this environment tends to have distinct multi-path characteristics [21] [22], for instance due to surface reflection of the signal. Shallow water noise also follows distinct patterns because of various noise sources [23], such as winds and shipping activity.

Design choices that address these challenges affect the battery lifetime of the network, which is our main metric of interest. The network battery life must be sufficiently long to avoid recharging or replacing node batteries frequently. A related metric that can be formulated is the power consumption to throughput ratio (*PCTR*), indicating the power cost of transmitting bits in the network.

Maximizing battery lifetime while minimizing *PCTR* typically requires networks to have less frequent data updates, lower spatial density, or shorter range [11]. All of these characteristics yield lower accuracy in the sensed data. Thus, there is a tradeoff involved between prolonging network lifetime and maximizing the accuracy of sensed data.

Consequently, the first step in our network battery life estimation method is to identify the design parameters that impact battery lifetime and power consumption, which are highly dependent on the network scenario. Next, the method investigates the signal propagation characteristics in the deployment region of interest as a

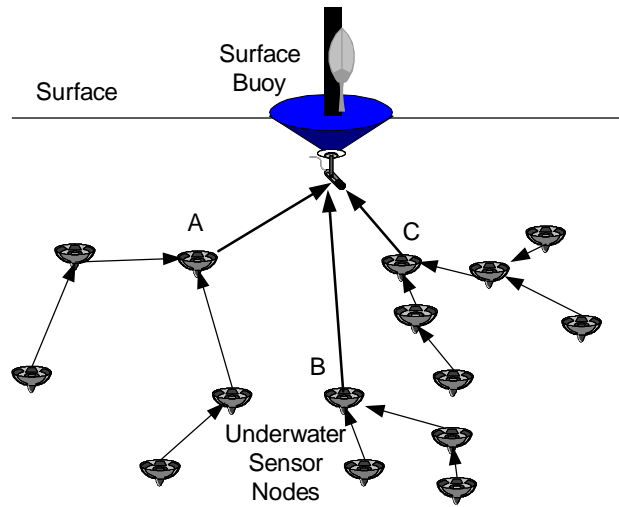


Figure 1.1. Example Underwater Sensor Network

function of the independent variables to derive the required transmission power for successful data reception. Third, we exploit the fact that data dissemination in our network is periodic and we compute the power cost of data delivery during one update period. Finally, the method uses the data delivery power cost during an update period to estimate the battery lifetime and power cost of the network. Each of the remaining subsections in this section focuses on one of these steps.

1.4.1 Network Design Parameters

Figure 1.1. illustrates our generalized network topology to analyze the tradeoffs of accurate underwater environmental indicator monitoring and power efficiency. The network in Figure 1.1. has a multi-hop centralized topology in which several trees are rooted at the base station, and data flow is always toward the base station. The convergence of data at the base station is appropriate for underwater sensor networks because sensor data in these networks is typically sent to shore for collection and analysis.

In the topology of Figure 1.1., nodes monitor their surrounding environmental conditions, and periodically send the collected information towards a central shore or surface station, which subsequently collects and processes the data. We consider the transmit and receive power to be the main sources of power consumption at each node [2] [20], and we assume that the sensing and processing powers are negligible.

Channel allocation is trivial for sparse networks since the data updates can be scheduled so that all nodes can use the same frequency channel at different times. However, as the network density increases, nodes must tightly synchronize their transmissions to avoid collisions on the common channel. Requiring tight synchronization among sensors adds implementation and communication cost to the network. Thus in the case of fairly dense networks, the first challenge is to provide a multiple access technique that does not rely on node synchronization and

that allows simultaneous transmissions by several nodes. We consider frequency division multiplexing as a multiple access technique for our method. Because the transmissions of nodes are separated through distinct frequency channels, a node A that uses a channel with a higher frequency consumes more power than a node B using a lower frequency channel because underwater signal propagation depends on both frequency and distance (see Section 1.4.2.2). As a result, the battery resources at A run out earlier than the resources at B. Thus, the maximum frequency (f) in any spectrum allocation scheme determines the worst case for battery lifetime and power consumption of the network.

Another factor that impacts network battery lifetime and power consumption is the frequency of data updates from sensors. One reasonable technique to prolong battery life is to increase the update period (R), which yields a lower power consumption rate. Significant variations in underwater medium conditions occur on the scale of a few minutes to the scale of decades [24] [25]. For example, managing a recreational beach area requires measuring danger from currents and wave sizes every several minutes. In contrast, coastal zone pollution management requires measurements in the time scale of years. Thus, an update period in the order of 20 minutes is sufficient to capture the environmental variations that occur in the shorter timescale.

To avoid consuming power for sending signals over long distances, we consider a multi-hop topology in which nodes that are closer to the base station¹ forward the signals of nodes further away from the base station (see Figure 1.1.).

As such, nodes that are further away from the base station need only consume transmit power to get the signal to the next hop. Thus, the inter-node distance (d) (or the length of one hop) has significant impact on power considerations of a multi-hop network. A multi-hop topology extends the range of operation of the network, but it raises the issue of increased power overhead at intermediate nodes, which have to forward the data of nodes further away. For example, if traffic routing is based solely on distance, then the nodes closest to the base station must forward the data of all the other nodes in the network. As such, it is important that the power costs of forwarding do not overburden the forwarding nodes.

To address this issue, nodes are divided into clusters that are defined by proximity. Within each cluster, nodes are segmented into tiers. Figure 1.2. shows a network topology with four clusters and three tiers per cluster. The nodes at the lowest tier (tier 3 in Figure 1.2.) are the furthest away from the base station and transmit messages to other nodes in the same cluster at the next higher tier (tier 2); tier 1 nodes, which are closest to the base station, finally transmit the accumulated data to the base station. Therefore, tier 1 nodes represent the bottlenecks in terms of battery lifetime, because they carry the burden of transmitting the messages of all other nodes in their respective clusters. Thus, the number of nodes in a cluster (M) is an important design choice of the network. The choice of M depends on the data sampling granularity that the application requires. M also establishes a tradeoff between the power consumption for transmissions over large distances and the power overhead of forwarding data. Note that forwarding nodes could aggregate or fuse their own data [26] with data arriving from more distant nodes in order to compress the overall amount of data to be transmitted, and, ultimately, to save on

¹A base station could be mounted on a surface buoy or on a nearby location on shore

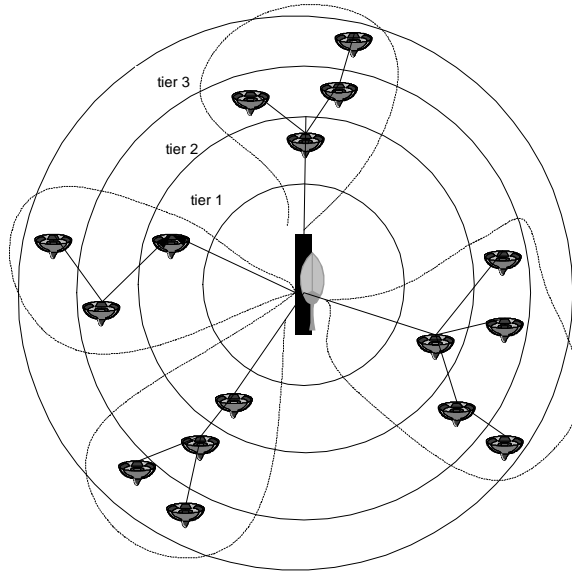


Figure 1.2. A network with four clusters and three tiers

transmission power. Our method does not consider aggregation, and thus presents a conservative estimate of the power consumption at the forwarding nodes.

In sum, we identified four important network design parameters that impact the battery lifetime and power consumption of an underwater sensor network: (1) the transmission frequency f ; (2) the update period R ; (3) the average signal transmission distance d ; and (4) the number of nodes in a cluster M .

1.4.2 Underwater Acoustics Fundamentals

1.4.2.1 The Passive Sonar Equation The passive sonar equation [4] characterizes the signal to noise ratio (SNR) of an emitted underwater signal at the receiver:

$$SNR = SL - TL - NL + DI \quad (1.1)$$

where SL is the source level, TL is the transmission loss, NL is the noise level, and DI is the directivity index. All the quantities in Equation 1.1 are in dB *re* μPa , where the reference value of $1 \mu Pa$ amounts to $0.67 \times 10^{-22} \text{ Watts/cm}^2$ [4]. In the rest of the paper, we use the shorthand notation of dB to signify dB *re* μPa .

Factors contributing to the noise level NL in shallow water networks include waves, shipping traffic, wind level, biological noise, seaquakes and volcanic activity, and the impact of each of these factors on NL depends on the particular setting. For instance, shipping activity may dominate noise figures in bays or ports, while water currents are the primary noise source in rivers. For the purpose of this analysis, we examined several studies of shallow water noise measurements under different conditions [23] [4]. As a result, we consider an average value for the ambient noise level NL to be 70 dB as a representative shallow water case. We also consider a target SNR of 15 dB [4] at the receiver.

The directivity index DI for our network is zero because we assume omnidirectional hydrophones. Note that this is another conservative assumption, since using a directive hydrophone as described in [10] reduces power consumption.

Through the above assumptions, we can express the source level SL intensity as a function of TL only:

$$SL = TL + 85 \quad (1.2)$$

in dB .

1.4.2.2 Transmission Loss The transmitted signal pattern has been modelled in various ways, ranging from a cylindrical pattern to a spherical one. Acoustic signals in shallow waters propagate within a cylinder bounded by the water surface and the sea floor, so cylindrical spreading applies for shallow waters. Urick [4] provides the following equation to approximate the transmission loss for cylindrically spread signals:

$$TL = 10 \log d + \alpha d \times 10^{-3} \quad (1.3)$$

where d is the distance between source and receiver in meters, α is the frequency dependent medium absorption coefficient, and TL is in dB .

Equation 1.3 indicates that the transmitted acoustic signal loses energy as it travels through the underwater medium, mainly due to distance dependent attenuation and frequency dependent medium absorption. Fisher and Simmons [27] conducted measurements of medium absorption in shallow seawater at temperatures of $4^\circ C$ and $20^\circ C$. We derive the average of the two measurements in Equation 1.4, which expresses the average medium absorption at temperatures between $4^\circ C$ and $20^\circ C$:

$$\alpha = \begin{cases} 0.0601 \times f^{0.8552} & 1 \leq f \leq 6 \\ 9.7888 \times f^{1.7885} \times 10^{-3} & 7 \leq f \leq 20 \\ 0.3026 \times f - 3.7933 & 20 \leq f \leq 35 \\ 0.504 \times f - 11.2 & 35 \leq f \leq 50 \end{cases} \quad (1.4)$$

where f is in Khz, and α is in dB/Km .

Through Equation 1.4, we can compute medium absorption for any frequency range of interest. We use this value for determining the transmission loss at various internode distances through Equation 1.3 which enables us to compute the source level in Equation 1.2 and subsequently to compute the power needed at the transmitter.

1.4.2.3 Transmission Power We have shown how the source level SL relates to internode distance and frequency through Equations 1.2, 1.3 and 1.4. SL also relates to the transmitted signal intensity at 1 m from the source according to the following expression:

$$SL = 10 \log \frac{I_t}{1 \mu Pa} \quad (1.5)$$

where I_t is in μPa . Solving for I_t yields:

$$I_t = 10^{SL/10} \times 0.67 \times 10^{-18} \quad (1.6)$$

in $Watts/m^2$, where the constant converts μPa into $Watts/m^2$.

Finally, the transmitter power P_t needed to achieve an intensity I_t at a distance of 1 m from the source in the direction of the receiver is expressed as [4]:

$$P_t = 2\pi \times 1m \times H \times I_t \quad (1.7)$$

in Watts, where H is the water depth in m.

In short, we have presented a method to obtain the required transmitter power for signal transmissions at a given distance d and frequency f . First, we can compute the transmission loss TL in terms of f and d and we subsequently compute the source level SL , which yields the source intensity I_t . Finally, we can compute the corresponding transmit power P_t needed to achieve a source intensity of I_t .

1.4.3 Data Delivery

We now present the tier-independent method for the estimation of battery lifetime and power consumption. In section 1.5 we consider more sophisticated tier-dependent frequency and distance assignments that build on the tier-independent method.

Without loss of generality, we assume that the size of data packets is 1 Kbit, which is enough to report 16 8-byte measurements, such as temperature, pressure, and salinity at every node in a 20 minute interval. We also assume that the bandwidth of each acoustic channel is 1 Khz. Thus, the available bit rate for each node is 1 Kbit/sec, which is well within the bit rates of current hydrophones [19], and the packet transmission time is 1 second. P_t is thus the power needed to transmit one packet in a contention-less environment. Note that a bandwidth of 1 Khz could be achieved through a combination of spread spectrum and frequency division multiplexing to achieve a higher number of coexisting nodes. Even if these multiple access techniques are used, packet collisions and corruptions remain possible. Furthermore, in each update period, a node not only sends its own data, but also the data of other nodes that are further away from a data sink.

We consider a generic Medium Access Control (MAC) protocol where a node accesses the channel, sends a data packet, and awaits an acknowledgement, which has a size of 200 bits. In the case that the acknowledgement times out, the node retransmits the data packet. Assuming a 0.1 packet loss rate, then each data packet and each acknowledgement is correctly received with a probability of 0.9. Consequently, the probability that both a packet and its corresponding acknowledgement are correctly received is 0.81, implying that each packet must be sent $1/0.81 = 1.23$ times on average. The node consumes power for sending and receiving data packets, as well as sending and receiving acknowledgments. The receive power of each message is typically around one fifth of the transmit power in commercially available hydrophones [19]. Thus, the average power in Watts consumed by a node during each update period (frame) is:

$$P_{frame} = 1.23P_t \times N \left(1 + \frac{1}{5} + \frac{1}{5} + \frac{1}{25} \right) \quad (1.8)$$

where N is the number of data packets that the node forwards during an update period. The first two terms in Equation 1.8 account for sending and receiving data packets, while the last two terms account for sending and receiving acknowledgments.

This paper considers two specific cases of cluster organizations: a linear chain, which represents the worst case scenario for network lifetime and applies to environmental monitoring along coastlines, rivers or aqueducts; and a grid topology, which applies to other practical environmental monitoring applications such as in a lake or bay. In the rest of this section, the discussion focuses on the chain topology,

and in Section 1.6.3, we apply the method to sensors placed in a grid topology. In the chain architecture, the average number of packets N forwarded by a node is equal to $M/2$ ².

As mentioned earlier, tier 1 nodes represent the bottleneck for network battery life, since they have the highest forwarding burden of all nodes. Thus, we express the maximum amount of power consumed during one frame at a tier 1 node as:

$$P_{max} = 1.23P_t \times N_{max} \left(1 + \frac{1}{5} + \frac{1}{5} + \frac{1}{25}\right) \quad (1.9)$$

in Watts, where N_{max} is the maximum number of packets forwarded by a tier 1 node. In the chain architecture, tier 1 nodes send their own data packet and forward the packets of all other nodes in the cluster during each update period, so N_{max} for this architecture is equal to M .

1.4.4 Network Lifetime and Power Consumption

A good measure of overall network power consumption is the ratio of overall power consumption to throughput. During each update period, each node in a cluster of M nodes sends its own data packet and forwards any pending data packets of its neighbors, yielding an average *PCTR* of:

$$PCTR = \frac{M \times P_{frame}}{M \times 1000 \text{ bits}} = \frac{P_{frame}}{1000} \quad (1.10)$$

in Watts/bit. Next we want to determine the limit on the battery lifetime of a network, which depends mainly on tier 1 nodes. The time that a node's transceiver is active during one update period is important for battery life considerations. Each node uses a store and forward mechanism to forward a sequence of packets as it receives them in order to minimize the active time of its transceiver. Taking into account collisions and retransmissions, the total active time for a tier 1 transceiver in one update period is:

$$T_{total} = 1.23 \left(N_{max} + \frac{N_{max}}{5} \right) \quad (1.11)$$

in seconds.

The next step is selecting a power source. We consider that we have 3 off-the-shelf 9V, 1.2 Amp-Hour batteries at each node. The total energy available at each node is:

$$E_t = 3 \times 9 \times 1.2 = 32.4 \quad (1.12)$$

in $V \cdot A \cdot \text{hour}$. The total active time of a transceiver is therefore the ratio of the total energy to the power consumed in one frame:

$$T_{active} = \frac{E_t}{P_{frame}} = \frac{32.4}{P_{frame}} \quad (1.13)$$

in hours. A node's transceiver is only active for a fraction of the time in each update period of R seconds. Therefore, the battery lifetime of a node is expressed by:

$$T_{lifetime} = \frac{T_{active}}{T_{total}} \times \frac{R}{24} \quad (1.14)$$

in days, where R is in seconds.

²This is a conservative estimate.

1.5 TOPOLOGY-DEPENDENT OPTIMIZATIONS

The tier-independent battery life and power consumption estimation method in Section 1.4 treats all network nodes equally, by assuming all internode distances are the same and by assigning frequency values randomly. However, the tier-independent method disregards the fact that tier 1 nodes carry a heavier power burden than other nodes. Consequently, applying measures that favor tier 1 nodes can yield improvements in battery life and power consumption. For this purpose, we propose two enhancements to the tier-independent battery life and power consumption estimation method: (A) tier-dependent frequency assignment; (B) tier-dependent distance assignment.

1.5.1 Tier-dependent Frequency Assignment

Equations 1.3 and 1.4 indicate that the transmission loss increases at higher frequencies, which implies that nodes using high frequencies must transmit acoustic signals at higher power. Thus, we assign tier 1 nodes the lowest frequency band, and we assign each subsequent tier the next higher frequency band, until nodes at the lowest tier are assigned the highest frequency band. This assignment allows nodes with higher forwarding load to use lower frequencies and thus save power.

1.5.2 Tier-dependent Distance Assignment

Equation 1.3 also shows that distance is the other independent variable that impacts transmission loss. Therefore, it would be beneficial to assign distances in a way that reduces the power load on nodes at lower tiers. Thus, we place tier 1 nodes at the shortest internode distance from the base station, and we increase internode distance for each subsequent tier.

1.5.3 Required Modifications

One goal of tier-dependent assignments is to reduce the overall power consumption per frame in the network. Thus, tier-dependent assignments require modifications to Equations 1.8, 1.9 and 1.11 in the general method, where N becomes:

$$N = M - i + 1 \quad (1.15)$$

for each tier i . As a result, P_{frame} , P_{max} , and T_{total} should be computed for each tier individually. We also modify the expression for $PCTR$ to reflect the distinction among tiers:

$$PCTR = \frac{\sum_{i=1}^M P_{frame}^i}{M \times 1000} \quad (1.16)$$

in Watts/bit, where P_{frame}^i is the power that a node at tier i consumes during one update period.

The other goal of tier-dependent assignments is to move the bottleneck tier away from the base station. Thus, equations 1.13 and 1.14 use the individual tier values for P_{frame} and T_{total} to compute the battery lifetime of each tier. This modification shifts the dependence of the network battery lifetime from tier 1 to the bottleneck tier i .

1.6 CASE STUDY

The requirements of our underwater environmental sensor network effort provided concrete values for some of the parameters discussed above. The deployment region of the network has a maximum depth of 10 m. To effectively monitor environmental indicators in the water, the recommended internode distances are in the range of 50 m to 1 km. The update period R is 20 minutes. Furthermore, maintenance work (such as cleaning) must be performed on the sensors themselves every 100 days or so, suggesting a target battery life of 100 days.

In the tier-independent method, we establish bounds for other parameters and analyze the results within those bounds. The maximum frequency varies from 1 KHz to 50 KHz, in steps of 1 KHz³. The maximum separation distance, which was established to be between 50 m and 1 Km, is increased in steps of 50 m. Finally, we consider that a set of M nodes are communicating within a cluster, where M varies from 1 to 500 with a step of 1.

The rest of this section is as follows. We first derive the $PCTR$ and battery lifetime of the chain topology for each combination of distance, frequency, and cluster size using the tier-independent method. Then, we derive results for the tier-dependent assignment methods and we compare them to the tier-independent method. Finally, we estimate and compare the battery life and power consumption for a grid topology using the tier-independent and frequency-dependent methods.

1.6.1 Tier-independent method

Figure 1.3. shows the power consumption to throughput ratio ($PCTR$) plotted in terms of the maximum frequency and internode distance for a cluster size of 500 nodes. The $PCTR$ increases with higher transmission frequencies at internode distances above 250 m, whereas frequency has little effect on $PCTR$ at distances below 250 m. The maximal impact of frequency on $PCTR$ can be seen at an internode distance of 1 Km, where transmission frequencies of 1 KHz and 50 KHz exhibit $PCTR$ values of 5.7 $\mu\text{W}/\text{bit}$ and 148 $\mu\text{W}/\text{bit}$ respectively. In contrast, varying internode distances from 50 m to 1 km does cause $PCTR$ to increase for both low and high frequencies, with the sharpest increase of $PCTR$ with distance occurring at 50 KHz.

Figure 1.4. illustrates the variation of the network battery lifetime according to the internode distance and the maximum frequency. The network battery life decreases sharply with increasing distance. When internode distances are small and the nodes transmit at low frequencies, the impact of medium absorption is negligible and most of the consumed power is due to signal attenuation (Equation 1.3). Medium absorption plays a larger role as the transmission frequency increases above 10 KHz resulting in shorter battery life. Transmitting at high frequencies over large distances shortens the battery life even further.

³This is in line with the capabilities of existing hardware.

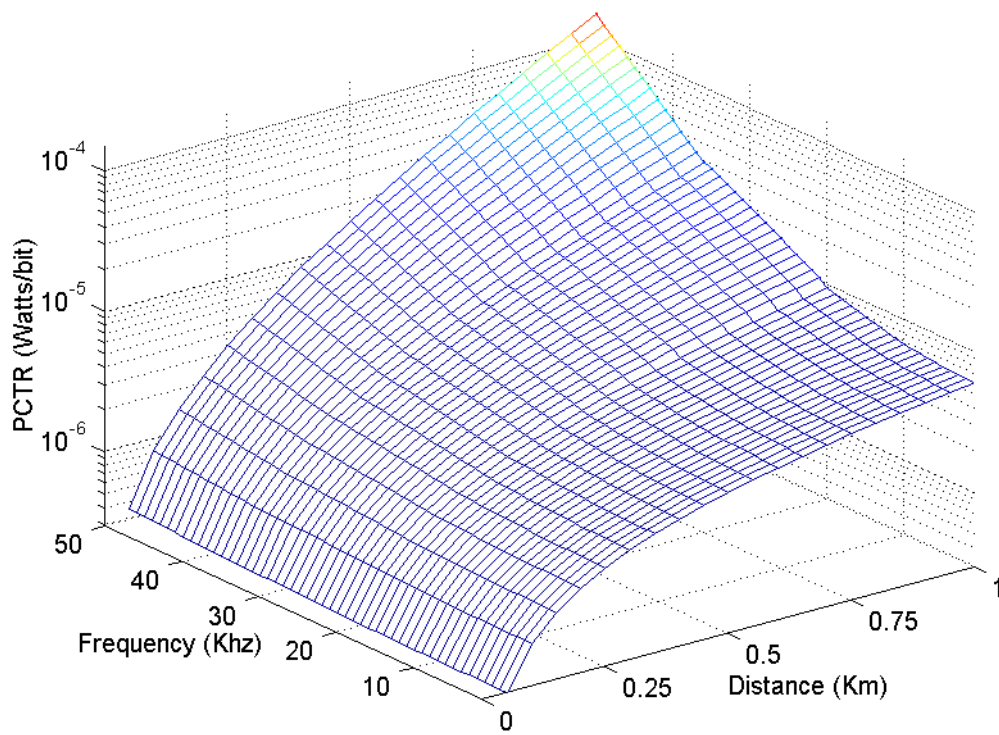


Figure 1.3. PCTR vs. Distance and Frequency, for a cluster size of 500 nodes

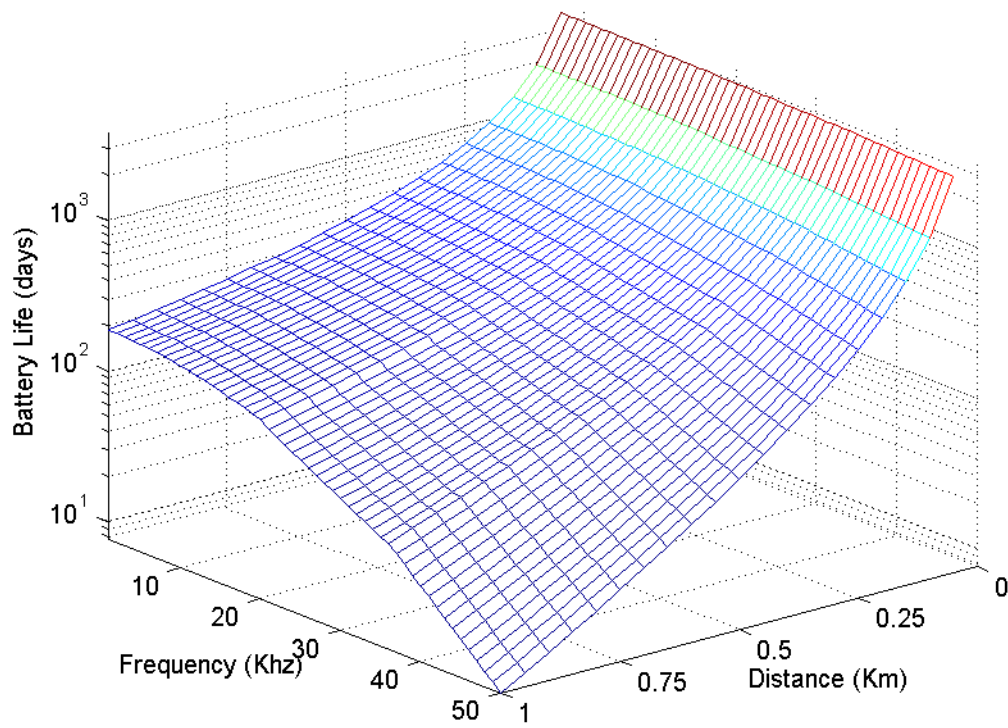


Figure 1.4. Network Battery Life vs. Distance and Frequency for a cluster size of 500 nodes

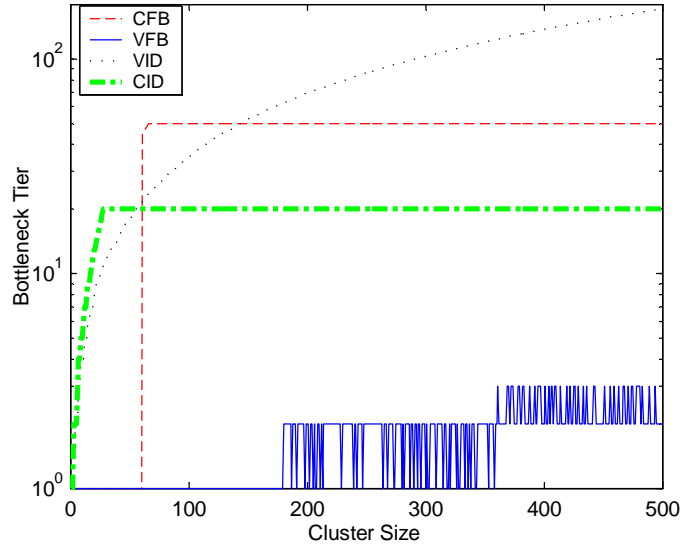


Figure 1.5. Bottleneck Tier vs. Cluster Size: the plots for the distance dependent cases are for a frequency of 50 KHz, and the plots for frequency dependent cases are for a distance of 1 Km

1.6.2 Tier-dependent Assignments

Now we derive results for the tier-dependent assignment methods in order to compare them with the tier-independent method. Within the tier-dependent frequency assignment, we consider two subcases:

1. Constant Frequency Band (CFB): we assign tier i nodes a frequency of i KHz, as long as i is less than 50. For values of i greater than 50, all tiers use a frequency of 50 KHz.
2. Variable Frequency Bands (VFB): frequency assignments for VFB are the same as CFB for cluster sizes within 50 nodes. For cluster sizes above 50, we divide up the spectrum into bands of $50/M$, and we assign the lowest frequency band to tier 1 nodes. Each subsequent tier uses the next higher frequency band.

Similarly, tier-dependent distance assignment has 2 subcases:

1. constant internode distance (CID): the internode distance of tier i is $50i$ meters for i less than 20, and 1 Km for the remaining tiers.
2. variable internode distances (VID): Internode distances in VID for cluster sizes below 20 are the same as for CID. For cases in VID where the cluster size is greater than 20, the increase in internode distance as we move up one tier is $1/M$ Km.

Figure 1.5. provides insight into the impact of tier-dependent assignments on the tier with the shortest battery lifetime (bottleneck tier). The bottleneck tier in the Constant Frequency Band method remains at tier 1 for cluster sizes below 60 nodes.

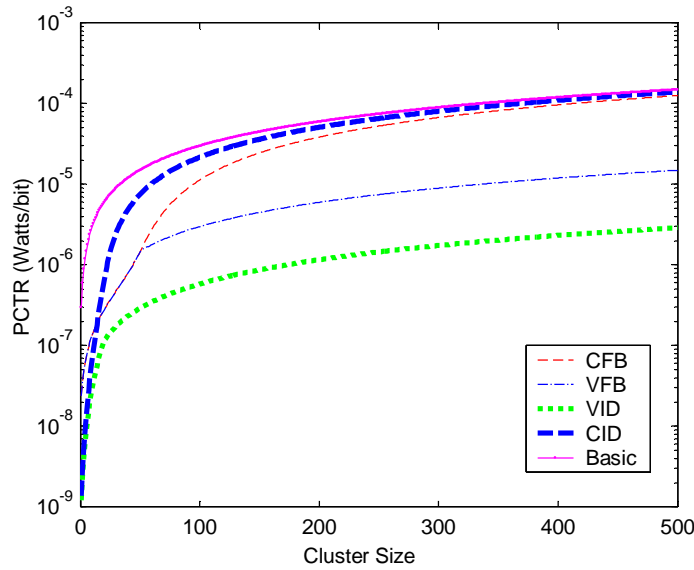


Figure 1.6. *PCTR* vs. Cluster Size: The plot for the tier-independent method shows *PCTR* for a distance of 1 Km and a frequency of 50 Khz. The plots for the frequency dependent assignments show *PCTR* for an internode distance of 1 Km, and the plots for the distance dependent assignments show the *PCTR* for a frequency of 50 Khz.

For higher cluster sizes, tier 50 becomes the bottleneck tier since nodes at tier 50 are both using the 50 Khz band (which has the highest power cost) and forwarding the data packets of other nodes. In the Variable Frequency Band method, the bottleneck tier remains at 1 for small cluster sizes, fluctuates between tiers 1 and 2 for moderate cluster sizes, and between tiers 2 and 3 for larger cluster sizes. The bottleneck tier remains close to the base station since only nodes furthest away from the base station are using the highest frequency bands. The bottleneck tier for Constant Internode Distances exhibits a similar behavior to CFB. The bottleneck tier shifts from tier 1 to tier 20 and remains there once the cluster sizes starts to grow. In the case of Variable Internode Distances, the bottleneck tier continues moving away from the base station as M increases to 500, and for a cluster size of 500 nodes, tier 227 is the bottleneck tier.

Figure 1.6. shows the variations of the *PCTR* for the tier-independent, CFB, VFB, CID, and VID cases as a function of M . The *PCTR* in the tier-independent case increases linearly with M as a direct consequence of Equations 1.8 and 1.10. For the Constant Frequency Band case, *PCTR* increases at a lower rate for small cluster sizes, where the maximum frequency in the network is less than 50 Khz. At cluster sizes above 50 nodes, *PCTR* for the Constant Frequency Band case increases linearly at the same rate as the tier-independent case, since each additional tier uses the frequency of 50 Khz and thus contributes a constant portion of additional power. The two plots converge for large cluster sizes. In the case of Variable Frequency Bands, the *PCTR* is the same as CFB for cluster sizes below 50 nodes. However, the *PCTR* for Variable Frequency Bands increases at a lower rate for cluster sizes larger than 50 nodes because VFB uses smaller frequency bands to accommodate additional tiers.

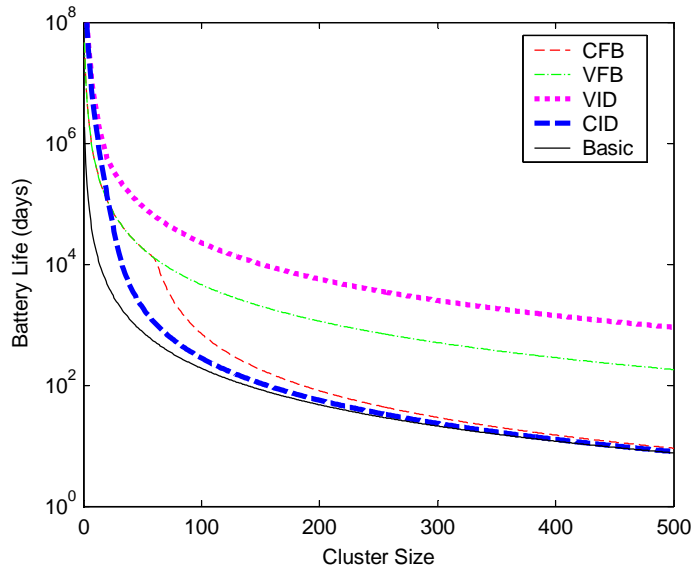


Figure 1.7. Network Battery life vs. Cluster Size: The plot for the tier-independent method shows $PCTR$ for a distance of 1 Km and a frequency of 50 Khz. The plots for the frequency dependent assignments show $PCTR$ for an internode distance of 1 Km, and the plots for the distance dependent assignments show the $PCTR$ for a frequency of 50 Khz.

The average power consumption for the Constant Internode Distance method is lower than the frequency dependent cases only for cluster sizes below 14 nodes. For larger cluster sizes, CID achieves less power savings than the frequency dependent methods, but still improves on the tier-independent case. $PCTR$ in the CID case increases linearly at about the same rate as Constant Frequency Band and the tier-independent case, since each additional tier has an internode distance of 1 Km and thus contributes a constant portion of additional power. As a result, the $PCTR$ of the Constant Internode Distances method converges with that of CFB and the tier-independent method for large clusters. Finally, the plot for the Variable Internode Distance case exhibits the lowest $PCTR$ of all cases. It follows the same behavior as CID for cluster sizes within 20, and then it increases slowly towards $3 \mu\text{W}/\text{bit}$ for 500 node clusters. As in the Variable Frequency Band case, the slower rate of increase in $PCTR$ for the Variable Internode Distance case stems from its use of smaller distance increments as the cluster size increases.

Figure 1.7. shows the variation of the network battery life as a function of cluster size using each of the five methods. The results in Figure 1.7. are a natural extension of the results in Figure 1.6.. Both CID and CFB yield a longer battery life than the tier-independent case for smaller cluster sizes. The battery life for CID drops more steeply than the battery life for CFB for smaller clusters, but the two plots converge together with the plot of the tier-independent method for high cluster sizes. The improvements in battery life for VFB and VID are more significant. For a cluster size of 500 nodes, Variable Frequency Bands yield a 24-fold improvement in network battery life, whereas Variable Internode Distances prolong the battery life by 131 times compared to the tier-independent method. The ratio of battery life for VID and VFB remains around 5 for medium and large cluster sizes.

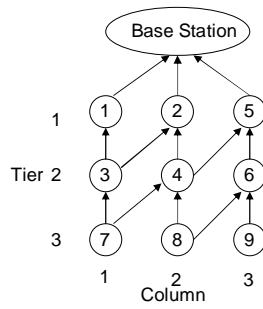


Figure 1.8. A grid topology network with 9 nodes: The indices of nodes indicate the order in which the nodes are added to expand the network. The arrows indicate the possible forwarding paths for each node.

1.6.3 Grid Topology

The estimation method uses the same equations for the grid topology as the ones for the chain topology, except for the values of N_{max} and N . In an $S \times S$ grid, N_{max} takes the value of S and N takes the value of $(S + 1)/2$.

Figure 1.8. illustrates a typical grid topology of 9 nodes. The node indices indicate the order in which nodes are placed in the grid coverage area. Once nodes form a perfect square, we begin adding sensors on tier 1 in a new column, then at tier 2, and so on, until we reach the highest tier. In Figure 1.8., once the first 4 nodes are in place, nodes 5 and 6 are added at tiers 1 and 2 in column 3. Once all existing tiers have a sensor in the new column, any additional sensors are placed in a new tier from left to right, until we get another perfect square topology.

Within the grid topology, nodes self-organize into a triangular lattice, as shown in Figure 1.8.. This architecture allows two nodes with the same child to share the load of forwarding that child's data. Load sharing is beneficial when one of the two parent nodes has fewer children than the other, since the parent nodes can take turns in forwarding the common child's data packets.

We estimate and compare the battery life and power consumption of the grid topology network for the tier-independent and the tier-dependent frequency assignment methods. Because the main application of a grid topology is environmental monitoring at uniform distances, we do not consider tier-dependent distance assignments for this topology.

Figure 1.9. shows the average power consumption in the network as the cluster size grows. An interesting observation of Figure 1.9. is the local maxima at perfect square cluster sizes. For those cases, the forwarding load is evenly split among the nodes of each tier, so load sharing does not yield any benefits. Adding an extra node to a perfect square network at tier 1 enables load sharing among the nodes of tier 1, which yields lower overall average power consumption. There are also local maxima in the plot of the frequency-dependent method at cluster sizes that correspond to a rectangular grid of size $k \times (k + 1)$ for any k . To explain these local maxima, consider again Figure 1.8. for $k = 2$. There are 6 nodes in the network, with three in each tier. This symmetry among nodes of the same tier reduces the benefits of load sharing as in the perfect square case. The ratio of battery life of the tier-dependent frequency method to the tier-independent method remains constant with

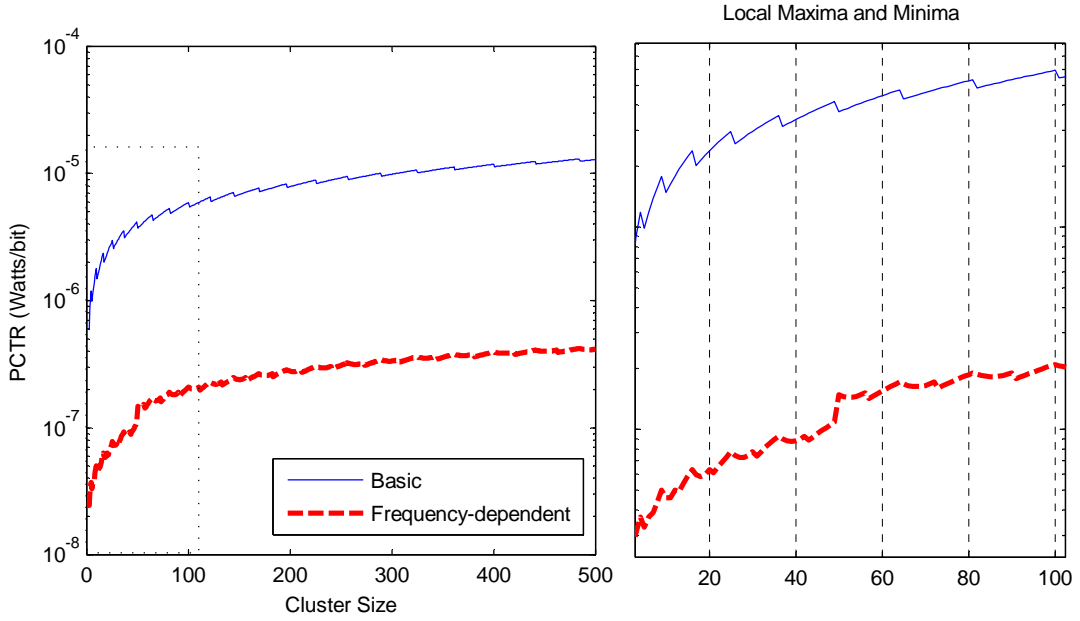


Figure 1.9. PCTR vs. Cluster Size for the grid topology: The plot for the tier-independent method shows $PCTR$ for a distance of 1 Km and a frequency of 50 KHz. The plot for the frequency dependent assignments show $PCTR$ for an internode distance of 1 Km.

a 30-fold improvement for cluster sizes larger than 50. The power savings that the tier-dependent frequency method achieves over the tier-independent method grow from $0.58 \mu\text{Watts/bit}$ for small clusters to $12.5 \mu\text{Watts/bit}$ for 500 node clusters.

Figure 1.10. shows the network battery life for the tier-independent and tier-dependent frequency methods as the cluster size grows. The local minima in the plots correspond to the perfect square cluster sizes, where the power consumption peaks (Figure 1.9.). In the tier-independent method, battery lifetime also drops steeply whenever adding a node corresponds to creating a new tier. In contrast, the tier-dependent frequency method does not have sharp drops for creating new tiers, primarily because tiers with high forwarding load use lower frequency bands, so the impact of nodes at a new tier is minimal. The tier-dependent frequency assignment method prolongs the battery life of the tier-independent method by a factor of 15. Even for large cluster sizes of 500 nodes in a $22 \times 22 \text{ Km}^2$ area, the battery life for both the tier-independent and tier-dependent methods is in the order of years, which is a significant improvement over the chain topology. This effect stems from the fact that in the grid topology, a fewer number of packets need to be forwarded by low tier nodes and neighboring nodes at the same tier can benefit from load sharing.

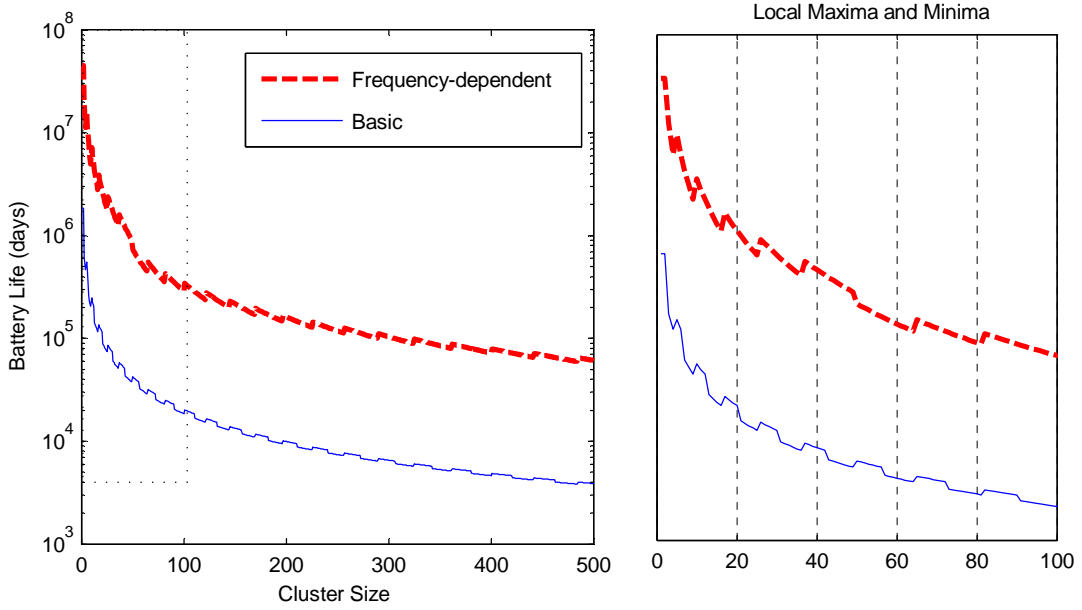


Figure 1.10. Battery Life vs. Cluster Size for the grid topology: The plot for the tier-independent method shows *PCTR* for a distance of 1 Km and a frequency of 50 KHz. The plot for the frequency dependent assignments show *PCTR* for an internode distance of 1 Km.

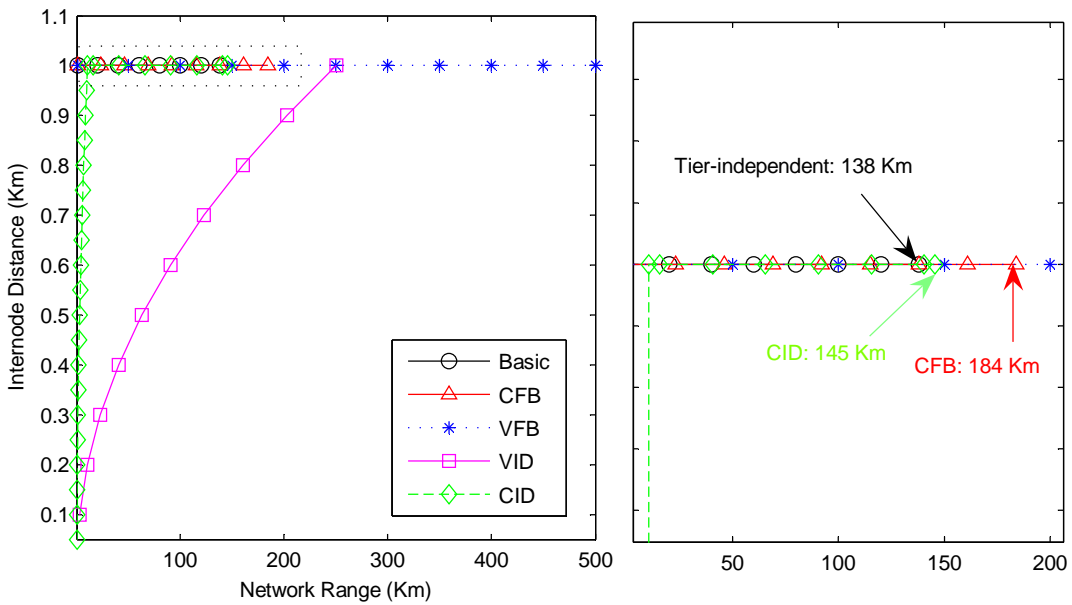


Figure 1.11. Internode distance vs. Network Range for a battery lifetime of 100 days

1.7 DISCUSSION AND CONCLUSION

1.7.1 Maximum Range Alternatives

One of the requirements of our particular shallow water network is that the sensor nodes should be retrieved and cleaned every 100 days or so. This requirement implies that the network battery lifetime must be at least 100 days. We can derive the options for achieving the target battery life for the chain topology from Figure 1.7..

The options that achieve the target battery life of 100 days are shown in Figure 1.11.. The right side of Figure 1.11. shows a magnified view of the overlapping plots in the left side. Using the tier-independent method limits M to 138 nodes per cluster, which provides a network range of 138 Km with a density of 1 node/Km. The Constant Internode Distance method achieves a slightly higher network range of 145 Km, with a cluster size of 155 nodes. The node density for CID decreases steadily from 20 nodes/Km to 1 node/Km for the first 20 tiers, and it remains at 1 node/Km for the remaining tiers. The Constant Frequency Band method supports 184 nodes per cluster for a battery life of 100 days, and as a result it further extends the network range to 184 Km with a density of 1 node/Km. For Variable Internode Distances, the node density decreases steadily from 500 nodes/Km at tier 1 to 1 node/Km at tier 500, achieving a network range of 250.5 Km. The Variable Frequency Band method achieves the highest network range of 500 Km, with a cluster size of 500 nodes and a density of 1 node/Km. Compared to the tier-independent method, VFB increases the cluster size, network range, and aggregated sensor data by a factor of 3.5. If we prolong the maintenance cycle to 1 year instead of 100 days, the cluster sizes of CFB, CID, VID, VFB and the tier-independent method drop to 120, 89, 500, 358, and 72 respectively.

In the grid topology, both the tier-independent and the tier-dependent frequency method achieve a battery life of more than a year for 500 node cluster sizes, with a density of 1 node/Km and a coverage area of $22 \times 22 \text{ Km}^2$.

1.7.2 Method Comparison

As the results in Figure 1.11. indicate, tier-dependent distance assignments provide fine-grained sampling of areas that are closer to the base station and less granular data in areas further away. For example, these methods are suitable for networks that require granular coastal data and coarser data from waters beyond coastal areas. In theory, Variable Internode Distance appears to provide for the longest battery life among the five methods considered. However, if nodes cannot be easily anchored at the sea floor at specific distances, then waves may move the sensors and as a result, the sensors would have to continuously discover distances from neighbors in order to adjust the transmit power accordingly. Furthermore, as cluster size increases, it becomes more difficult and expensive to realize the shorter internode distances and larger number of sensors that VID requires. The Constant Internode Distance method improves on the tier-independent method, but it has a shorter battery life and a shorter range than VID, VFB and CFB. However, CID has looser requirements on node placement than VID, which makes it more practical. Since only the first 20 nodes in CID are placed at progressively increasing distances, it is easier and cheaper to place these 20 nodes at the specified distances and subsequently place all other nodes at large approximate distances.

Tier-dependent frequency assignments have looser sensor placement requirements and provide data with uniform granularity. Thus, both frequency assignment methods are suitable for many environmental applications that require sampling of underwater data at regular distance intervals or for applications that tolerate approximate sensor placement. Frequency dependent assignments are also suitable for self-organizing sensor networks in which the sensors must discover the topology themselves and choose frequency bands according to their position in the topology. Constant Frequency Bands add only minimal complexity to the tier-independent scheme by requiring that nodes are aware of their position in the topology in order to choose an appropriate frequency. The Variable Frequency Band method, which achieves the longest network range, adds more signal processing complexity, since it requires the same channel rate using a smaller frequency bandwidth.

1.7.3 Grid Topology

Applying the estimation methods to a grid topology with uniformly placed nodes yielded longer network lifetime than all cases of the converging chain network, which is to be expected since the chain topology represents the lower bound on network lifetime. As mentioned earlier, networks with a grid topology are useful for environmental monitoring of lakes or bays. The estimation results that we derived cover a maximum area of $22 \times 22 \text{ Km}^2$. To apply the results to larger areas, a relay station at the edge of each cluster can collect the data and forward to the base station. Alternatively, the network can still use a single base station and simply expand cluster sizes to cover the larger area.

1.7.4 Self-recharging Sensors

Battery lifetime in sensor networks becomes less of an issue if there is some way of recharging battery resources at individual nodes without human intervention. In an underwater sensor network, nodes can derive mechanical, chemical, or solar energy from their surrounding environment. For example, nodes could absorb and store mechanical energy from water flows through small windmill-like devices. Whether the benefits of such devices outweigh the cost of building them into sensor nodes remains an open issue.

1.7.5 Method Applicability

Although we applied our method to a shallow seawater network, the method also applies to networks at any depth and any fluid. In deeper waters, the impact of both distance and frequency on transmission loss changes. One obvious distinction is that the signal undergoes spherical spreading for deeper waters, as opposed to cylindrical spreading in shallow water. Medium absorption is also depth dependent, and several studies [28] have explored this dependence through measurements. Other factors, such as the noise level, should also be modified to represent deep water environments. Applying the method to other fluids also requires similar changes to the path loss and noise models. Finally, the network deployment setting may require other changes to the method. For instance, there is no signal spreading in pipes and the transmission loss beyond a certain range is independent of distance.

Conclusion In sum, we derived a method to estimate the battery life and power cost for underwater sensor networks. Our method first identifies the main independent variables (f , d , M , R) that impact network battery life and power consumption. Next, the method investigates the signal propagation characteristics in the deployment region of interest as a function of the independent variables (f and d in this case) to derive the required transmission power for successful data reception. Third, the transmission power estimate is combined with the relevant independent variables (M and R in this case) to compute the power cost of data delivery during one update period. Finally, the method uses the data delivery power cost during an update period to estimate the average node battery life and average network power cost.

We applied this estimation method and its tier-dependent variants to a set of shallow water network scenarios which are representative of our underwater sensor network effort. We found that for the chain topology, the Variable Internode Distance method achieves the longest battery life compared to the tier-independent and frequency assignment methods, and it provides better fine-grained sampling compared to the other methods for the same target battery life. On the other hand, the Variable Frequency Band method maximizes network range for a given cluster size, provides data samples at uniform granularity, and still achieves a comparatively long battery life.

We also applied the method to a grid topology with uniformly placed sensors to estimate the network battery life and power consumption. The battery life was expectedly longer in the grid topology than the chain topology, and the tier-dependent frequency assignments prolonged battery life nearly by a factor of fifteen over the tier-independent method. Because our method is applicable to any topology or fluid medium, researchers can adapt the method to estimate power consumption and network battery life in the initial design and planning stages of fluid sensor networks.

REFERENCES

1. National oceanic and atmospheric administration. available:<http://www.csc.noaa.gov/coos/hawaii.html>, 2003.
2. M. Bhardwaj, T. Garnett, and A.P. Chandrakasan. Upper bounds on the lifetime of sensor networks. In *International Conference on Communications*, volume 3, pages 785–790. IEEE, 2001.
3. J. Zhu and Symeon Papavassiliou. On the Energy-Efficient Organization and the Lifetime of Multi-hop Sensor Networks. *IEEE Communications Letters*, volume 7:11, pages 537–539, 2003.
4. R. J. Urick. *Principles of Underwater Sound*. Mcgraw-Hill, 1983.
5. J. Groen, J.C. Sabel and A. Htet. Synthetic aperture processing techniques applied to rail experiments with a mine hunting sonar. In Proc. *UDT Europe*, 2001.
6. P.T. Gough and D.W. Hawkins. A short history of synthetic aperture sonar. In Proc. *IEEE Int.Geoscience and Remote Sens. Symp.*, 1998.
7. P. Chapman, D. Wills, G. Brookes, and P. Stevens. Visualizing Underwater Environments Using Multi-frequency Sonar. In *IEEE Computer Graphics and Applications*, 1999.

8. G.M. Trimble. Underwater Object Recognition and Automatic Positioning to Support Dynamic Positioning. In *Proc 7th Int. Symposium Unmanned Untethered Submersible Technology*, pages 273–279, 1991.
9. X. Yang et al. Design of a Wireless Sensor Network for Longterm, In-Situ Monitoring of an Aqueous Environment. *Sensors*, 2:455-472, 2002.
10. N. Fruehauf and J.A. Rice. System design aspects of a steerable directional acoustic communications transducer for autonomous undersea systems. In *OCEANS*, volume 1, pages 565 –573. IEEE, 2000.
11. S. Tilaky, N. B. Abu-Ghazalehy, and W. Heinzelman. Infrastructure tradeoffs for sensor networks. In *WSNA*, 2002.
12. M.A. Marsan, C.F. Chiasserini, A. Nucci, G. Carello, and L. De Giovanni. Optimizing the topology of bluetooth wireless personal area networks. In *INFOCOM*, volume 2, pages 572 –579. IEEE, 2002.
13. A. Misra and S. Banerjee. Mrpc: maximizing network lifetime for reliable routing in wireless environments. In *Wireless Communications and Networking Conference*, volume 2, pages 800–806. IEEE, 2002.
14. J. H. Chang and L.Tassiulas. Energy conserving routing in wireless ad-hoc networks. In *Proc. Annual Joint Conference of the IEEE Computer and Communications Societies*, pages 22-31, 2000.
15. Y. Xu, J. Heidemann, and D. Estrin. Geography-informed energy conservation for ad hoc routing. In *Mobile Computing and Networking*, pages 70-84, 2001.
16. S. Lindsey and C. S. Raghavendra. Pegasus: Power-efficient gathering in sensor information systems. In *Proc. IEEE Aerospace Conference*, 2002.
17. W. Ye, J. Heidemann, and D. Estrin. An energy-efficient MAC protocol for wireless sensor networks. In *Proc. IEEE INFOCOM 02*, 2002.
18. D. Panigrahi, C. Chiasserini, S. Dey, R. Rao, A. Raghunathan, and K. Lahiri. Battery life estimation of mobile embedded systems. In *Fourteenth International Conference on VLSI Design*, pages 57 –63, 2001.
19. Underwater Acoustic Modem. available: www.link-quest.com.
20. K. Kalpakis, K. Dasgupta, and P. Namjoshi. Maximum lifetime data gathering and aggregation in wireless sensor networks. In *International Conference on Networking*, pages 685–696. IEEE, 2002.
21. J. G. Proakis, J.A. Rice, and M. Stojanovic. Shallow water acoustic networks. *IEEE Communications Magazine*, (11), 2001.
22. M. Stojanovic. Recent advances in high speed underwater acoustic communications. *Oceanic Engineering*, 21(4):125–36, 1996.
23. S. A. L. Glegg, R. Pirie, and A. LaVigne. A study of ambient noise in shallow water, available:<http://www.oe.fau.edu/acoustics/>.
24. A. B. Boehm, S. B. Grant, J. H. Kim, S. L. Mowbray, C. D. McGee, C. D. Clark, D. M. Foley, and D. E. Wellman. Decadal and shorter period variability of surf zone water quality at huntington beach, california. *Environmental Science and Technology*, 2000.
25. R. Holman, J. Stanley and T. Ozkan-Haller. Applying Video Sensor Networks to Nearshore Environment Monitoring. *Pervasive Computing*, pp. 14-21, 2003.
26. Z. Xinhua. An information model and method of feature fusion. In *ICSP*, 1998.
27. F. H. Fisher and V. P. Simmons. *Sound Absorption in Sea Water*. Journal of Acoustical Society of America. 62:558, 1977.
28. F. H. Fisher. *Effect of High Pressure on Sound Absorption and Chemical Equilibrium*. Journal of Acoustical Society of America. 30:442, 1958.